

## Development of a 3D QSAR Model for the Prediction of HDAC2 Inhibitory Activity

Dr. Faten Alchab\*  
Majd Mohamed\*\*

(Received 12 / 9 / 2024. Accepted 18 / 12 / 2024)

### □ ABSTRACT □

Histone Deacetylase 2 (HDAC2) plays an important role in various dangerous disease pathologies such as cancer, and was recently shown to be a desirable target for selective inhibition, thus multiple studies were conducted in an effort to develop potent selective HDAC2 inhibitors. This study focuses on developing a 3D QSAR model using a modified CoMSIA approach, in order to better determine inhibitory activity of novel compounds, while also providing a model to guide further inhibitor design and optimization. The models were generated using 168 carefully selected inhibitors from the literature, and were thereafter evaluated and validated through multiple parameters to determine the model with the best predictivity. The best generated model was then studied to identify important compound physiochemical properties that significantly affect inhibitory activity against HDAC2, and it was found that the presence of large bulky groups at the active site rim, together with an aromatic ring within the hydrophobic channel, enhance HDAC2 inhibitory activity.

**Keywords:** HDAC2, HDAC2 inhibitors, 3D QSAR, CoMSIA, Molecular docking.



Copyright :Tishreen University journal-Syria· The authors retain the copyright under a CC BY-NC-SA 04

\* Professor - Department of Pharmaceutical Chemistry and Drug Control, Faculty of pharmacy, Tishreen university, Latakia, Syria. [faten.alchab@tishreen.edu.sy](mailto:faten.alchab@tishreen.edu.sy)

\*\* MD Student – Department of Pharmaceutical Chemistry and Drug Control, Faculty of pharmacy, Tishreen university, Latakia, Syria. [majd.mohamed@tishreen.edu.sy](mailto:majd.mohamed@tishreen.edu.sy)

## تطوير نموذج QSAR ثلاثي الأبعاد للتنبؤ بالفعالية التثبيطية على أنزيم HDAC2

د. فاتن الشب\*  
مجد محمد\*\*

(تاريخ الإيداع 12 / 9 / 2024. قبل للنشر في 18 / 12 / 2024)

### □ ملخص □

أنزيم هيستون دي أسيتيلاز 2 (HDAC2) يلعب دوراً مهماً في تطور العديد من الأمراض الخطيرة مثل السرطان، وقد تبين مؤخراً أنه يشكل هدفاً مهماً للتثبيط الانتقائي من أجل تدبير وعلاج هذه الأمراض، ومنه اهتمت العديد من الدراسات بتطوير مثبطات انتقائية عالية الفعالية على HDAC2. تهتم هذه الدراسة بتطوير نموذج QSAR ثلاثي الأبعاد باستخدام مقارنة CoMSIA معدلة، من أجل تقييم الفعالية التثبيطية على HDAC2 للمركبات الدوائية الجديدة، بالإضافة إلى توليد نموذج يساهم في توجيه عملية تصميم وتحسين هذه المثبطات. تم توليد النماذج باستخدام 168 مثبط مختار بعناية من الأدبيات العلمية، ومن ثم تم تقييمها وتصديقها عبر معايير مناسبة من أجل تحديد النموذج ذو القدرة التنبؤية الأفضل. تم بعد ذلك دراسة النموذج الأفضل لتحديد الخصائص الفيزيائية والكيميائية التي تؤثر بشكل كبير على الفعالية التثبيطية، وتبين أن وجود مجموعة كبيرة الحجم عند مدخل الجيب الفعال، وحلقة عطرية ضمن القناة الكارهة للماء، تساهم في تحسين الفعالية التثبيطية على HDAC2.

**الكلمات المفتاحية:** HDAC2، مثبطات HDAC2، علاقة البنية بالفعالية الكمية ثلاثية الأبعاد، CoMISA، إرساء جزيئي

حقوق النشر: مجلة جامعة تشرين - سورية، يحتفظ المؤلفون بحقوق النشر بموجب الترخيص CC BY-NC-SA 04



\* مدرس - قسم الكيمياء الصيدلانية والمراقبة الدوائية، كلية الصيدلة، جامعة تشرين، اللاذقية، سوريا.

[faten.alchab@tishreen.edu.sy](mailto:faten.alchab@tishreen.edu.sy)

\*\* طالب ماجستير - قسم الكيمياء الصيدلانية والمراقبة الدوائية، كلية الصيدلة، جامعة تشرين، اللاذقية، سوريا.

[majid.mohamed@tishreen.edu.sy](mailto:majid.mohamed@tishreen.edu.sy)

## 1. Introduction:

Histone Deacetylase Enzymes are a family of intracellular enzymes that play a crucial role in cell cycle progression and proliferation, while also contributing to other significant biological functions. HDACs mechanism of action entails Post Translation Modification (PTM) on a variety of proteins, predominately chromosomal histones, through lysin  $\epsilon$  side chain deacetylation, affecting both gene translation and transcription. 18 human HDAC isoforms have been identified, 11 of which are zinc dependent, simply referred to as HDACs, while 7 are  $\text{NAD}^+$  dependent, referred to as Sirtuins. Zinc dependent Histone Deacetylase Enzymes have been intensively studied for the treatment and management of multiple diseases such as cancer [1-3]. HDAC2 in particular was recently shown to be a promising therapeutic target for multiple dangerous malignant, cardiovascular, neurodegenerative and muscular diseases [4, 5].

### 1.1. Histone Deacetylase 2 (HDAC2):

HDAC2 belongs to Class I of HDAC enzymes, and is found within the nucleus of all human cells, and plays a role in multiple disease pathologies through various branching mechanisms due to its high deacetylation potency over histones and other proteins. HDAC2 was found to be upregulated in various types of cancer such as liver, gastric, colorectal, bone and lung tumors [4], where it affects tumor prognosis through direct or indirect activation of specific oncogenes and pro-oncogenesis pathways such as the apoptosis inhibiting NF- $\kappa$ B pathway [6], or inhibition of tumor suppressor genes and proteins such as  $\text{p16}^{\text{INK4A}}/\text{p21}^{\text{WAF1/Cip1}}$  genes and p53 protein [7, 8]. HDAC2 was also found to be implicit in neurodegenerative diseases such as Alzheimer's due to its negative impact on synapsis elasticity and long-term memory formation [5, 9, 10]. Moreover, HDAC2 plays a role in cardiac hypertrophy due to glycogen synthase kinase 3b (Gsk3b) inhibition [11], and Duchenne Muscular Dystrophy (DMD) through indirect inhibition of follistatin [12].

HDAC2 active site consists of three main regions, namely the rim at the entrance of the active site pocket, followed by a hydrophobic channel, and then the catalytic acetate binding site. Additionally, HDAC2 active site also contains a region called the foot pocket situated deep within the pocket adjacent to the acetate binding site [13, 14]. Figure 1 illustrates the aforementioned regions, rim (blue), hydrophobic channel (yellow), acetate binding site (red), and foot pocket (green).

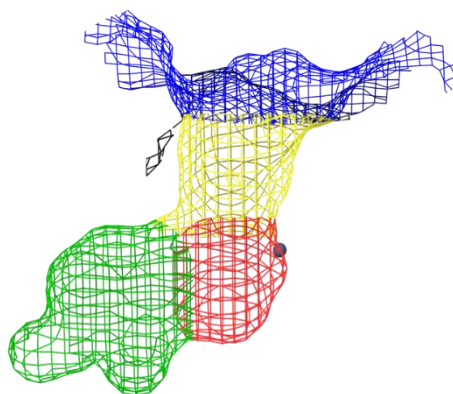


Figure 1: HDAC2 active site pocket regions

### 1.2. HDAC2 inhibition:

HDAC inhibition has proven to be an effective cancer treatment [15]. However, pan-HDAC inhibition is accompanied by potentially dangerous side effects such as cardiovascular and neurotoxicity [10, 16, 17], whereas HDAC2 selective inhibition could prove to be a better, more potent and less toxic alternative, while also having multiple therapeutic applications other than cancer due to its role in the aforementioned diseases [4, 5]. Unfortunately, there are no currently approved HDAC2 selective inhibitors. Thus, multiple HDAC2 selective inhibitors are currently being developed and studied through various molecular modelling approaches, and this study focuses on predicting the potency of potential HDAC2 inhibitors through building a 3D field-based QSAR model, in order to better determine inhibitory activity, and guide novel inhibitor design.

### 1.3. 3D QSAR:

The goal of 3D-QSAR is to establish the relationship between biological activity and spatial properties of the studied compounds such as steric, electrostatic, and lipophilic properties called descriptors. Multiple methods have been developed like MSA, CoMFA and CoMSIA, the latter being the one used in this study, as it offers distinguishing advantages benefitting this work [18].

Comparative Molecular Similarity Indices Analysis (or for short CoMSIA) is a ligand-based, alignment-dependent, and linear 3D-QSAR method, which relies mainly on calculating five similarity fields: steric, electrostatic, hydrophobic, hydrogen bond acceptor, and hydrogen bond donor for the aligned molecules, through interactions with an appropriate probe (charged atom for electrostatic, hydrogen bond donor and acceptor for the hydrogen bond fields and so on) situated at equally spaced grid points. These interactions are then used as descriptors which are correlated with biological data (inhibitory activity) using a Partial Least Square (PLS) approach in order to obtain a QSAR model, presented graphically as contour maps [19, 20].

The CoMSIA methodology enables ascertaining the importance of specific physiochemical properties (electrostatic, hydrophobic, hydrogen bonding, etc.) contributing to the activity model and their 3D spatial configuration relative to the ligand skeleton, while providing contour maps that are easy to interpret and could be further used to guide ligand modification through favorable and unfavorable ligand groups correspondence with each similarity field [18-20].

## 2. Materials and Methods:

The Schrodinger 2023.1 molecular modelling suite [21-24] was used to carry out this study.

### 2.1. Data set preparation:

Data set selection is a crucial step in building a QSAR model, as compounds used to build, test, and verify the model are the defining factor for its success and applicability. Thus, in order to build a model that is both predictive and has a large area of applicability, compounds were selected from previous studies and scientific literature based on the following criteria:

- All compounds are tested in-vitro using the same method to determine their experimental HDAC2 inhibitory activity
- Compounds with different structures and similar activities
- Compounds with similar structures and different activities
- Compounds spanning multiple magnitudes of activity
- Highly active compounds as they provide important structural information

The selected compounds were drawn in the 2D sketcher of the Maestro interface, and then prepared using the Ligprep module. The compounds were then separated into three sets: training, test, and external validation, while ensuring fair distribution of compounds in each set.

### 2.2. Compound alignment:

Alignment was performed through molecular docking into a prepared HDAC2 active site (PDB: 7KBG) using Glide XP docking protocol, this approach could help provide more insight into the effect of protein binding site interactions on overall inhibitory activity, and not solely relying on ligand-based descriptors.

The protein structure of HDAC2 (PDB: 7KBG) was retrieved from the RCSB database [25-28], and prepared using the protein preparation workflow module. Hydrogen atoms and missing loops were added. Zero-order bonds were assigned to metals. Missing side chains were filled. Energy minimization was performed (convergence RMSD threshold was  $0.3\text{\AA}$ ) using the OPLS4 force field [29], and water molecules were deleted as per recommendations from the software developer.

The Glide receptor grid that will be used for docking was generated using the appropriate residues as centre of the generated grid (GLY139, GLY150, PHE151, TYR304, ZN401). However, it has been shown that the internal cavity (foot pocket region) of HDAC2 undergoes significant structural changes during drug-receptor complex formation with compounds that can access said region [30, 31]. This change greatly impacts the ability of compounds to successfully dock in the active site. This will be simulated using the Induced Fit Docking protocol [32] in the Glide module which simulates residue flexibility by docking a known HDAC2 inhibitor 2-thienyl CI-994 [33]. The resulting complex will be used to generate the receptor grid.

The Glide XP docking protocol was then used to dock all compounds into the prepared HDAC2 active site.

### 2.3. Building and validating the QSAR models:

The 3D field-based QSAR from the Prime module was used to build the QSAR models using the aligned compounds, with different numbers of PLS factors, and each generated model was then evaluated and validated through multiple parameters. The Prime module uses a modified CoMSIA method for generating the models, and an extended Gaussian function was selected which uses an aromatic ring similarity field in addition to the aforementioned five fields. Grid spacing was set to  $1\text{\AA}$ , and number of ligands to leave out for cross validation was set to 1, the remaining parameters were set to default. Tables 1 and 2 present the parameters used for the internal evaluation of the models using the test set.

**Table 1: Parameters for the internal evaluation and validation of QSAR models**

Parameters	Description	Required value
Training set	SD	Standard deviation of the regression
	$R^2$	The coefficient of determination
	$R^2$ CV	Cross-validated $R^2$ value
	$R^2$ scramble	Average value of $R^2$ from a series of models built using scrambled activities
	Stability	Stability of the model predictions to changes in the training set composition
	F	Fisher coefficient
Test set	P	Statistical significance
	RMSE	Root-mean-square error
	$Q^2$	The coefficient of determination
	Pearson-r	Pearson r value for the correlation between the predicted and observed activity

Furthermore, to ensure good model predictivity, the external validation set of compounds was used to evaluate model predictability independently from model generation, according to the parameters set by Tropsha et al.[34-36]. These calculations were carried out using the Enalos module of KNIME software on the model with best internal validation results.

**Table 2: Parameters for the external validation of QSAR models**

Parameters	Description	Required value
$R^2$	The coefficient of determination	>0.6
$R^2_{CVEXT}$	The coefficient of determination after cross validation	>0.5
$(R^2 - R_0'^2)/R^2$	Ratio of conventional coefficient of correlation and coefficients of determination	<0.1
$(R^2 - R_0'^2)/R^2$		
$ R_0'^2 - R_0'^2 $	Absolute difference of coefficients of determination	<0.3
K	Slopes of the respective regression model	$0.85 < \_ < 1.15$
K'		

The model with the best accommodating parameters will be chosen as the best model.

### 3. Results and Discussion:

#### 3.1. Data set preparation:

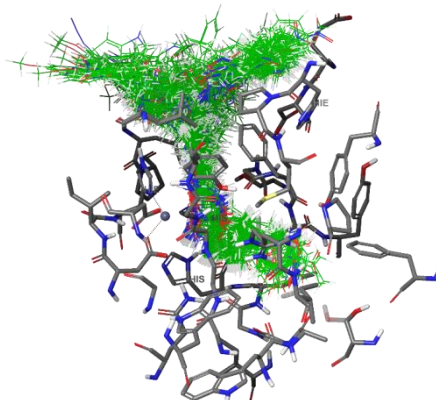
168 compounds were selected from appropriate studies and scientific literature [37-52] according to the previously mentioned parameters. The chosen compounds were split into training set (85 compounds) used to build the models, test set (34 compounds) used for internal evaluation, and validation set (49 compounds) used for external validation and had no part in model building. Tables 3-5 present the structure of the chosen compounds, with their respective inhibitory activity calculated using the formula:

$$Activity = pIC50 = -\log(IC50)$$

Compounds had an  $IC_{50}$  ranging from 3.5 nM to 100  $\mu$ M.

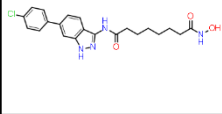
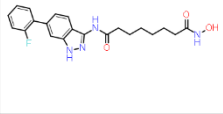
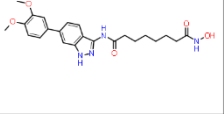
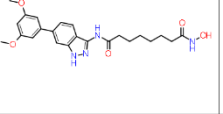
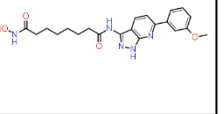
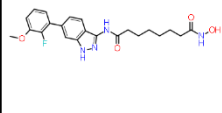
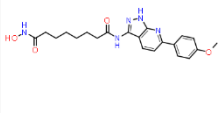
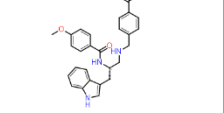
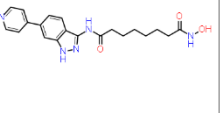
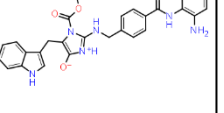
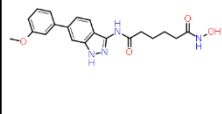
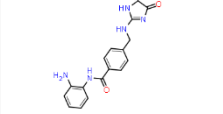
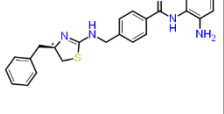
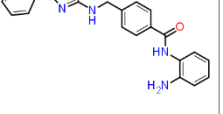
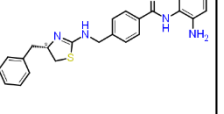
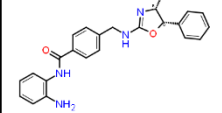
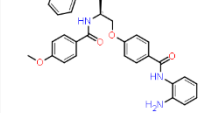
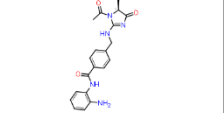
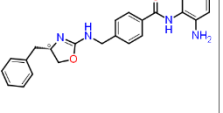
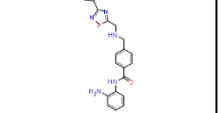
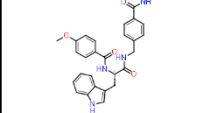
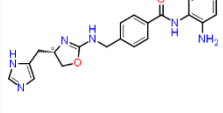
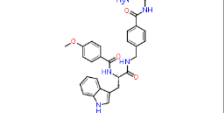
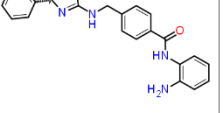
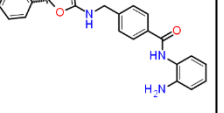
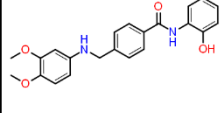
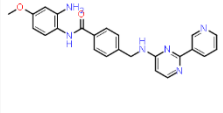
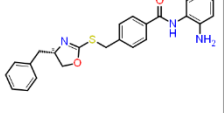
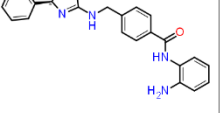
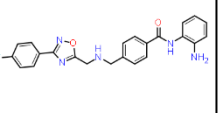
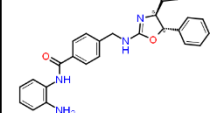
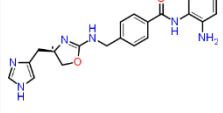
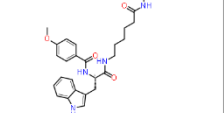
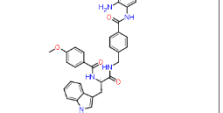
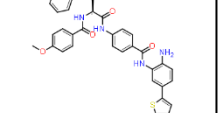
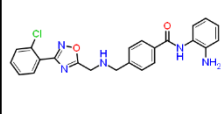
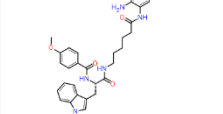
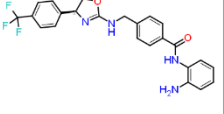
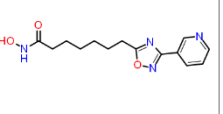
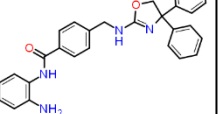
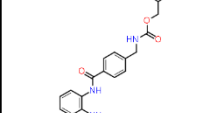
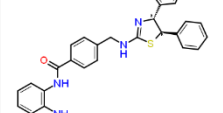
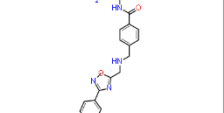
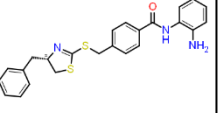
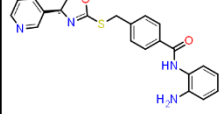
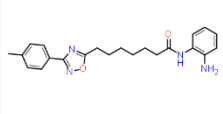
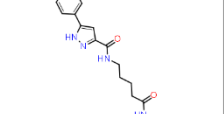
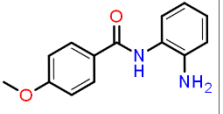
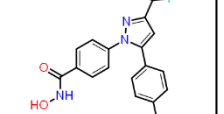
#### 3.1. Compound alignment:

Aligned compounds (green skeleton) within HDAC2 active site are presented in figure 2.



**Figure 2: Aligned compounds within HDAC2 active site**

Table 3: Chemical structures of the training set compounds

				
Activity 6444	Activity 6257	Activity 6337	Activity 6319	Activity 6276
				
Activity 6272	Activity 6066	Activity 7674	Activity 7587	Activity 7319
				
Activity 7388	Activity 7188	Activity 7666	Activity 7101	Activity 6983
				
Activity 6959	Activity 6955	Activity 6956	Activity 6956	Activity 6924
				
Activity 6936	Activity 6796	Activity 6267	Activity 6743	Activity 6717
				
Activity 6499	Activity 6066	Activity 6460	Activity 6569	Activity 6553
				
Activity 6553	Activity 6538	Activity 6528	Activity 6507	Activity 6503
				
Activity 6495	Activity 6471	Activity 6488	Activity 6499	Activity 6398
				
Activity 6387	Activity 6272	Activity 6276	Activity 6136	Activity 6237
				
Activity 6235	Activity 6107	Activity 6094	Activity 6165	Activity 6077

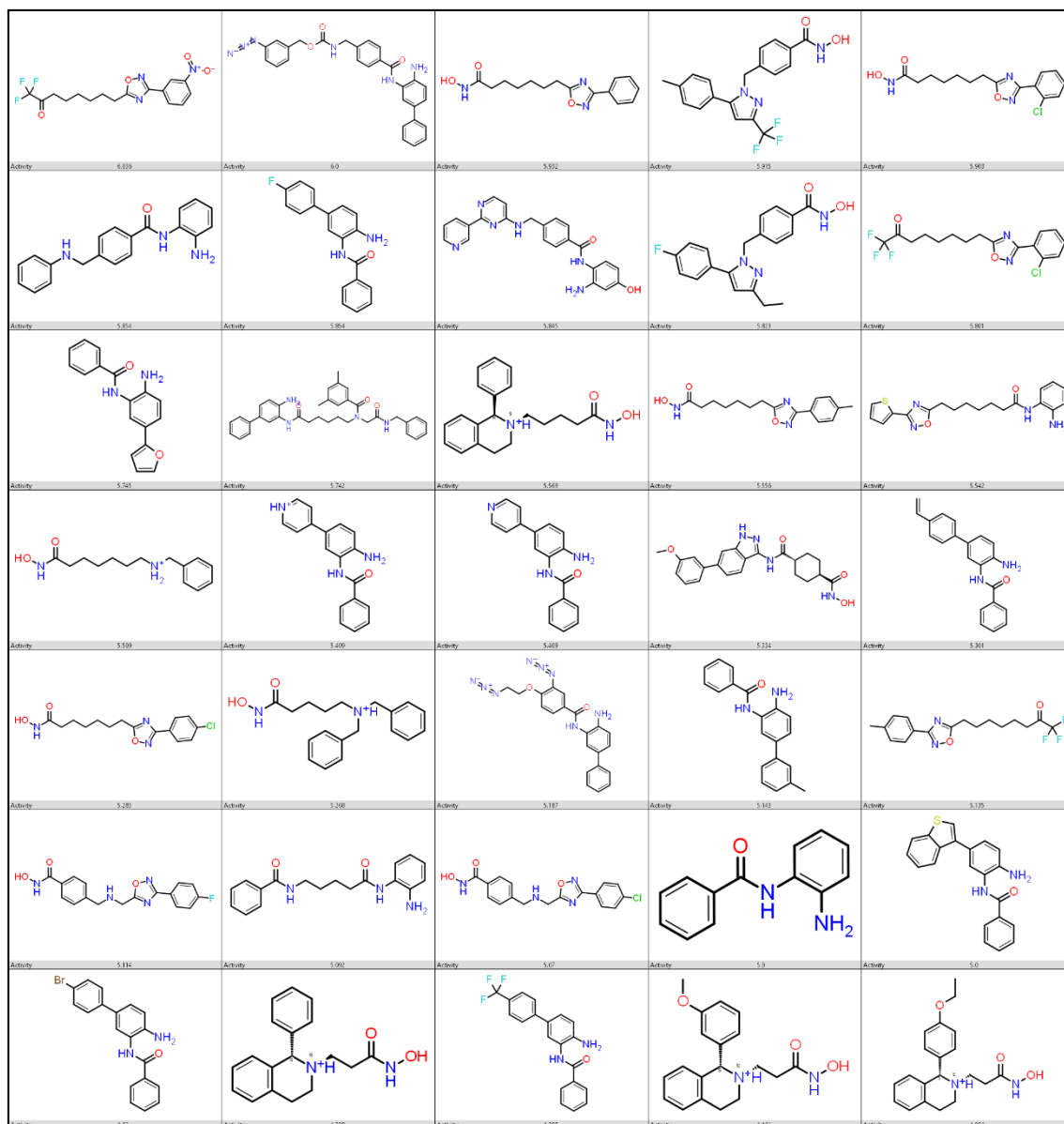
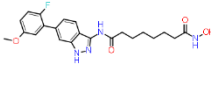
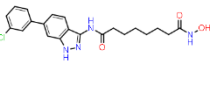
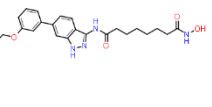
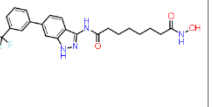
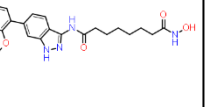
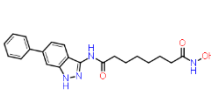
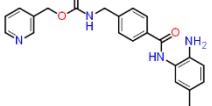
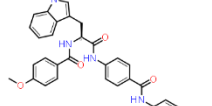
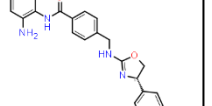
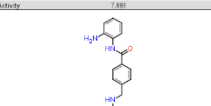
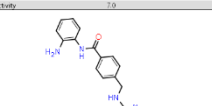
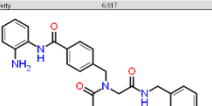
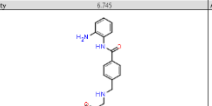
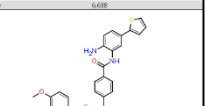
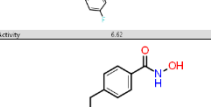
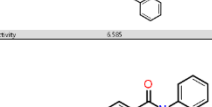
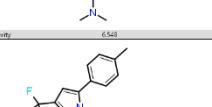
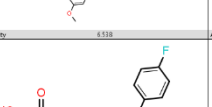
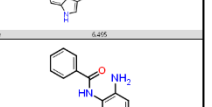
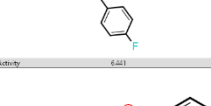
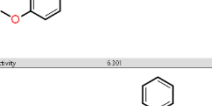
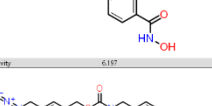
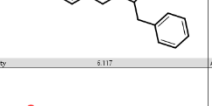
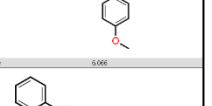
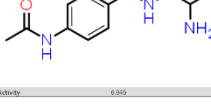
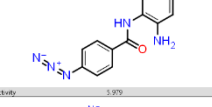
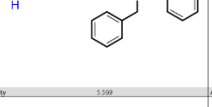
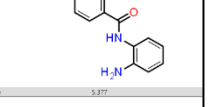
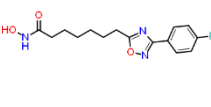
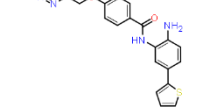
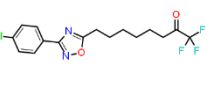
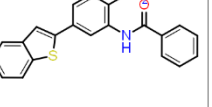
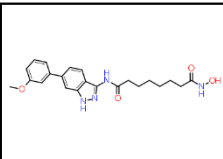
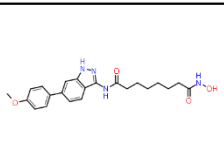
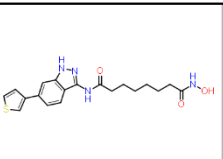
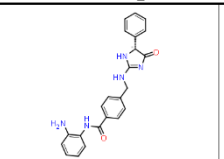
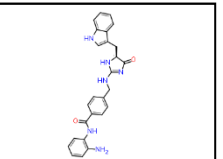
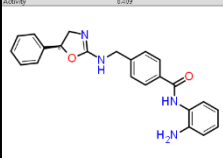
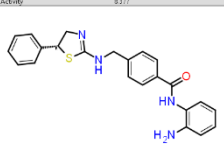
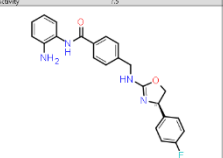
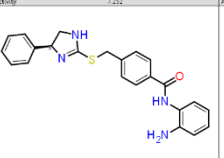
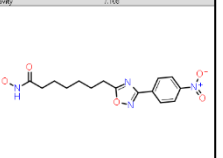
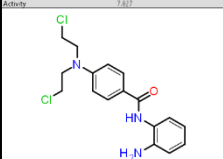
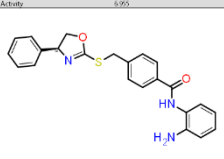
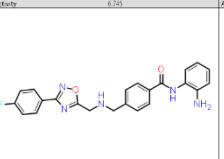
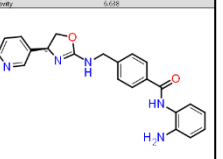
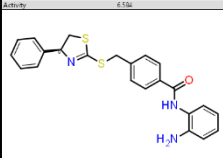
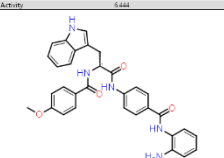
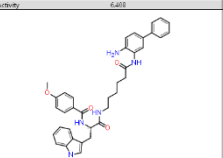
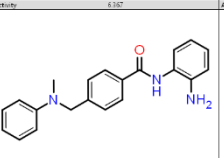
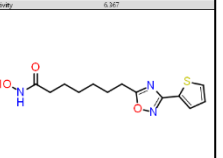
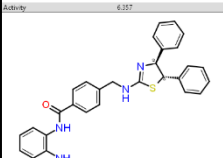
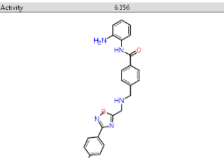
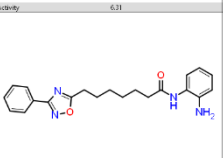
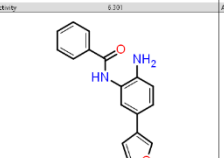
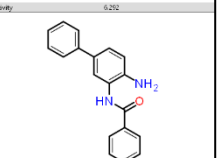
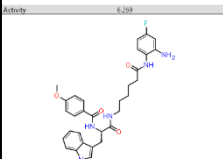
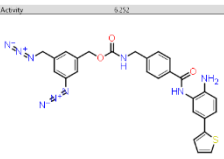
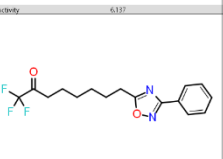
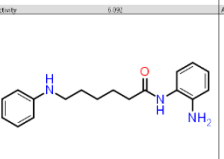
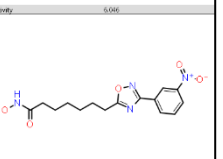
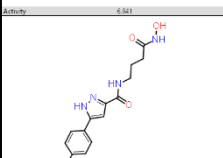
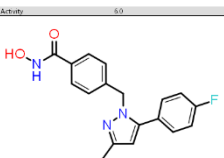
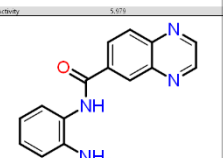
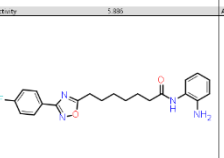
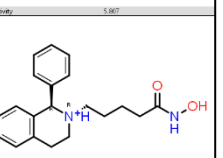
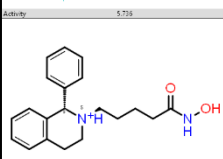
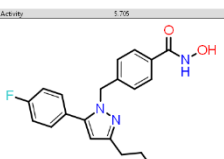
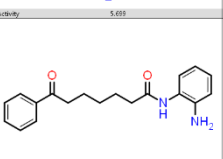
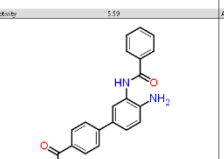
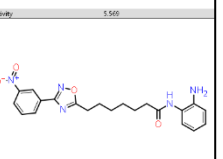
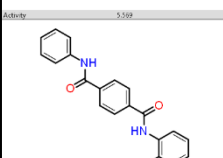
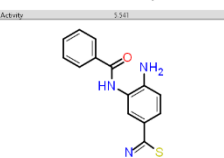
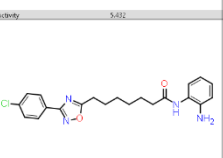
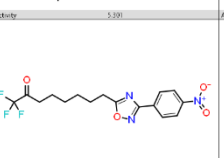
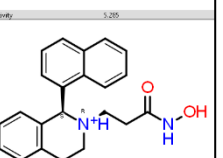
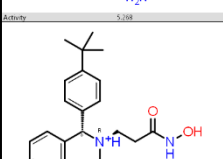
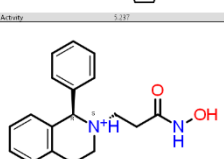
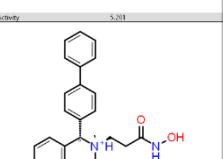
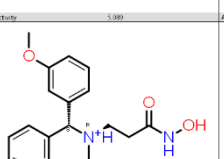


Table 4: Chemical structures of test set compounds

				
Activity 6456	Activity 6296	Activity 6377	Activity 6301	Activity 6266
				
Activity 7889	Activity 710	Activity 6977	Activity 6345	Activity 6698
				
Activity 641	Activity 6585	Activity 6548	Activity 6538	Activity 6495
				
Activity 6441	Activity 6301	Activity 6197	Activity 6117	Activity 6066
				
Activity 6385	Activity 6379	Activity 5954	Activity 5589	Activity 5377
				
Activity 5381	Activity 538	Activity 5164	Activity 518	Activity 510
				
Activity 4285	Activity 4536	Activity 4370	Activity 4277	

**Table 5: Chemical structures of validation set compounds**

				
Activity 6109	Activity 6177	Activity 75	Activity 7252	Activity 7166
				
Activity 7377	Activity 6995	Activity 6802	Activity 6751	Activity 6488
				
Activity 6584	Activity 6444	Activity 6488	Activity 6387	Activity 6347
				
Activity 6357	Activity 6356	Activity 631	Activity 6291	Activity 6292
				
Activity 6109	Activity 6292	Activity 6117	Activity 6196	Activity 6096
				
Activity 6541	Activity 610	Activity 5179	Activity 5386	Activity 5367
				
Activity 5753	Activity 5795	Activity 5689	Activity 519	Activity 5668
				
Activity 5168	Activity 5241	Activity 5432	Activity 5391	Activity 5285
				
Activity 5168	Activity 5127	Activity 5281	Activity 5389	Activity 4886
				
Activity 4759	Activity 4795	Activity 4823	Activity 4181	

### 3.1. Building and validating the QSAR models:

Three QSAR models were built using different numbers of PLS factors, table 6 presents the internal evaluation and validation parameters of the best generated models using one, two, and three PLS factors.

**Table 6: Internal evaluation and validation parameters of the generated models**

# Factors	SD	R <sup>2</sup>	R <sup>2</sup> CV	R <sup>2</sup> scramble	Stability	F	P	RMSE	Q <sup>2</sup>	Pearson-r
1	0.4365	0.8053	0.7144	0.162	0.97	343.2	3.16e-31	0.36	0.9055	0.9548
2	0.3305	0.8897	0.8345	0.3955	0.983	330.8	5.53e-40	0.38	0.8949	0.9481
3	0.2928	0.9145	0.8539	0.5169	0.983	288.8	3.87e-43	0.39	0.8933	0.9472

All models exhibited good parameters overall, with both high stability and test set experimental vs predicted activity correlation (Q<sup>2</sup>). However, models 2 and 3 showed better cross validation coefficients (R<sup>2</sup> CV) with the leave-one-out method, and since both models exhibited similar test set results and model 2 showed lower probability of fitting random data (R<sup>2</sup> scramble), model 2 was chosen as the best model due to having a lower chance of over-fitting. Further analysis on the external validation set using the Tropsha et al. parameters (figure 3) showed that model 2 shows good predictivity. Figure 4 represents experimental vs predicted activity plot for all three sets of compounds for model 2.

Criterion	Assessment	Result
R <sup>2</sup> > 0.6	PASS	R <sup>2</sup> = 0.719
R <sub>cv</sub> ext <sup>2</sup> > 0.5	PASS	R <sub>cv</sub> ext <sup>2</sup> = 0.73
(R <sup>2</sup> -R <sub>0</sub> <sup>2</sup> )/R <sup>2</sup> < 0.1	PASS	(R <sup>2</sup> -R <sub>0</sub> <sup>2</sup> )/R <sup>2</sup> = 0.085
(R <sup>2</sup> -R' <sub>0</sub> <sup>2</sup> )/R <sup>2</sup> < 0.1	PASS	(R <sup>2</sup> -R' <sub>0</sub> <sup>2</sup> )/R <sup>2</sup> = 0.006
abs(R <sub>0</sub> <sup>2</sup> -R' <sub>0</sub> <sup>2</sup> ) < 0.1	PASS	abs(R <sub>0</sub> <sup>2</sup> -R' <sub>0</sub> <sup>2</sup> ) = 0.057
0.85 < k < 1.15	PASS	k = 1.003
0.85 < k' < 1.15	PASS	k' = 0.991

**Model Predictive**

**Figure 3: External validation of model 2 using Tropsha et al. parameters**

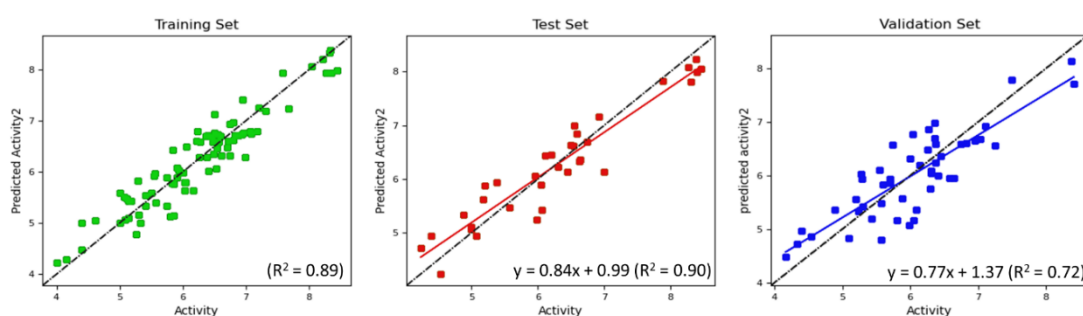


**Figure 4: Experimental vs predicted activity plot for model 2**

Tables 7-9 compare experimental vs predicted activity of all compounds.

**Table 7: experimental vs predicted activity of training set compounds**

#	Activity	Predicted												
1	8.444	7.993	18	6.936	6.751	35	6.503	7.130	52	6.000	6.143	69	5.334	5.136
2	8.357	7.971	19	6.886	6.727	36	6.495	6.357	53	5.932	5.991	70	5.301	5.391
3	8.337	8.403	20	6.824	6.752	37	6.471	6.618	54	5.915	5.960	71	5.285	5.839
4	8.319	8.319	21	6.804	6.881	38	6.469	6.660	55	5.903	5.859	72	5.268	4.589
5	8.276	7.949	22	6.796	6.613	39	6.409	5.967	56	5.854	5.837	73	5.187	5.631
6	8.222	8.229	23	6.747	6.896	40	6.398	6.690	57	5.854	5.373	74	5.143	5.343
7	8.046	8.086	24	6.745	6.399	41	6.387	6.356	58	5.845	6.469	75	5.135	5.536
8	7.674	7.206	25	6.717	6.658	42	6.372	6.732	59	5.823	5.738	76	5.114	5.615
9	7.587	7.967	26	6.699	6.475	43	6.276	6.654	60	5.801	5.049	77	5.092	5.077
10	7.319	7.118	27	6.606	6.348	44	6.260	6.211	61	5.745	5.545	78	5.070	5.663
11	7.208	7.343	28	6.602	6.723	45	6.237	6.841	62	5.742	5.924	79	5.000	5.739
12	7.180	6.870	29	6.569	6.609	46	6.215	6.646	63	5.569	5.259	80	5.000	5.255
13	7.086	6.770	30	6.553	6.781	47	6.167	5.461	64	5.556	5.934	81	4.620	5.291
14	7.071	6.811	31	6.553	6.664	48	6.054	6.559	65	5.542	5.951	82	4.398	5.259
15	6.983	6.323	32	6.538	6.559	49	6.046	5.933	66	5.509	5.460	83	4.398	4.330
16	6.959	6.729	33	6.529	5.979	50	6.037	5.571	67	5.409	5.750	84	4.161	4.236
17	6.955	7.387	34	6.507	6.752	51	6.036	5.672	68	5.409	5.563	85	4.004	4.194

As previously mentioned, this method ascertains which physiochemical properties are more relevant to predicted overall compound activity, this can be shown through table 10 as percentage of contribution, where it is apparent that steric similarity field had the highest contribution (37.6%), meaning that the shape and spatial positioning of the compound largely contribute to its activity, which is fairly common amongst drugs. Hydrophobic, hydrogen bond donor and acceptor, and aromatic ring fields had relatively similar contributions (11.3%-16.5%), while the electrostatic field showed the lowest contribution to overall activity (6.8%).

**Table 8: experimental vs predicted activity of test set compounds**

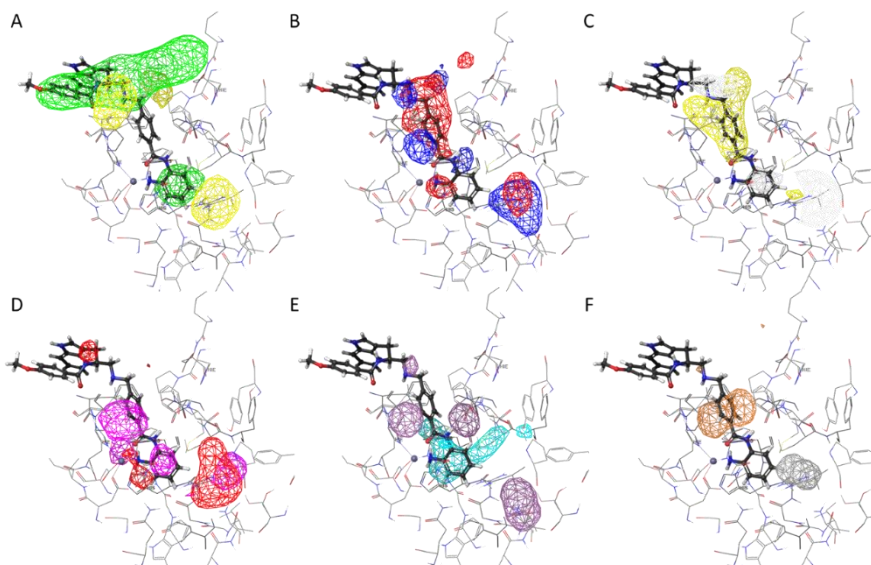
#	Activity	Predicted	#	Activity	Predicted	#	Activity	Predicted	#	Activity	Predicted	#	Activity	Predicted
1	8.456	8.030	8	6.917	7.081	15	6.495	6.628	22	5.979	5.471	29	5.000	5.344
2	8.398	8.017	9	6.745	6.737	16	6.441	6.039	23	5.959	6.203	30	5.000	5.318
3	8.377	8.291	10	6.638	6.476	17	6.301	6.271	24	5.569	5.257	31	4.886	5.049
4	8.301	7.856	11	6.620	6.385	18	6.197	6.311	25	5.377	5.970	32	4.538	4.185
5	8.268	8.074	12	6.585	6.931	19	6.117	6.311	26	5.203	5.840	33	4.398	4.715
6	7.883	7.815	13	6.548	6.991	20	6.066	5.635	27	5.180	5.758	34	4.237	4.600
7	7.000	6.272	14	6.538	6.689	21	6.046	5.978	28	5.068	4.986			

**Table 9: experimental vs predicted activity of validation set compounds**

#	Activity	Predicted												
1	8.409	7.712	11	6.584	5.949	21	6.269	6.856	31	5.736	6.574	41	5.268	6.033
2	8.377	8.135	12	6.444	6.358	22	6.252	6.476	32	5.705	5.933	42	5.237	5.332
3	7.500	7.793	13	6.408	5.998	23	6.137	6.195	33	5.699	5.866	43	5.201	5.553
4	7.252	6.565	14	6.367	6.244	24	6.092	5.363	34	5.590	5.833	44	5.089	4.835
5	7.108	6.930	15	6.367	6.589	25	6.046	5.162	35	5.569	4.795	45	4.886	5.353
6	7.027	6.673	16	6.357	6.702	26	6.041	6.773	36	5.569	5.476	46	4.538	4.854
7	6.955	6.652	17	6.356	6.980	27	6.000	6.317	37	5.541	6.105	47	4.398	4.960
8	6.824	6.597	18	6.310	6.049	28	5.979	5.068	38	5.432	5.190	48	4.328	4.725
9	6.745	6.594	19	6.301	6.083	29	5.886	5.565	39	5.301	5.421	49	4.161	4.480
10	6.638	5.956	20	6.292	5.754	30	5.807	5.157	40	5.285	5.937			

**Table 10: Similarity field contributions to overall predicted activity of model 2**

# Factors	Gaussian steric	Gaussian electrostatic	Gaussian hydrophobic	Gaussian hbond acceptor	Gaussian hbond donor	Gaussian aromatic ring
1	35.3	6.9	17.4	15.3	11.8	13
2	37.6	6.8	16.5	14.6	11.3	13
3	36.7	7	16.8	14.6	12	12.6

**Figure 5: QSAR model 2 field contours; steric (A), electrostatic (B), hydrophobic (C), hydrogen bond acceptor (D), hydrogen bond donor (E), aromatic ring (F)**

Model 2 field contours are shown in figure 5, overlaid on a training set compound (black skeleton) within the active site, and contour information are presented in table 11. A positive contour means that the presence of the corresponding physicochemical group or

function in this position is favorable to increase activity, while a negative contour means that its presence is unfavorable and could lead to lower activity, except for electrostatic where positive and negative are indicative of the corresponding charge.

**Table 11: QSAR model 2 contours description**

<b>Similarity field contours</b>	<b>Positive</b>	<b>Negative</b>
Gaussian Steric	Green	Yellow
Gaussian Electrostatic	Blue	Red
Gaussian Hydrophobic	Yellow	White
Gaussian Hbond Acceptor	Red	Magenta
Gaussian Hbond Donor	Purple	Cyan
Gaussian Aromatic Ring	Orange	Gray

By analyzing the previous contours, it is apparent that according to model 2 the inhibitory activity increases significantly by the presence of bulky groups at the rim (entrance) of the active site, and also increases with the presence of hydrophobic groups within the hydrophobic channel area, which is somewhat expected as this channel houses the hydrophobic lysine side chain throughout the deacetylation process [2]. Additionally, the presence of an aromatic ring in the hydrophobic channel, and a hydrogen bond acceptor and donor deep within the foot pocket also serve to increase activity. On the other hand, the presence of bulky or aromatic groups in the foot pocket, hydrogen bond acceptors in the hydrophobic channel, or hydrogen bond donors in the acetate binding site, all diminish activity. These findings are in accordance with previous studies on Class I HDACs [53, 54]. Looking back at the compounds used to generate and validate the model, we find that the more active compounds all have large bulky groups that would be positioned at the rim of the active site pocket, while less active compounds are generally smaller and thus more confined to the hydrophobic channel. Figure 6A illustrates a comparison between two compounds with similar scaffolds, however they differ in their interaction with the rim, where the more active compound (green skeleton) has a large group positioned within this region, while the smaller less potent compound (purple skeleton) lacks such a group, and this could explain the large difference in experimental activity ( $IC_{50} = 21$  nM vs 4600 nM respectively). Hydroxamic acid compounds benefit from the fact that they don't occupy the foot pocket and thus are better positioned to interact with the rim with their bulky groups, whereas benzamides are situated deeper within the active site and occupy the foot pocket with an aromatic ring or a larger group, and thus have to be larger themselves (higher molecular weight) in order to interact with the rim in a similar manner. Figure 6B illustrates this points by comparing the positioning of both a hydroxamic acid compound (yellow skeleton) and a benzamide (green skeleton) with similar experimental activities ( $IC_{50} = 25.9$  nM vs 21 nM respectively) within the HDAC2 active site.

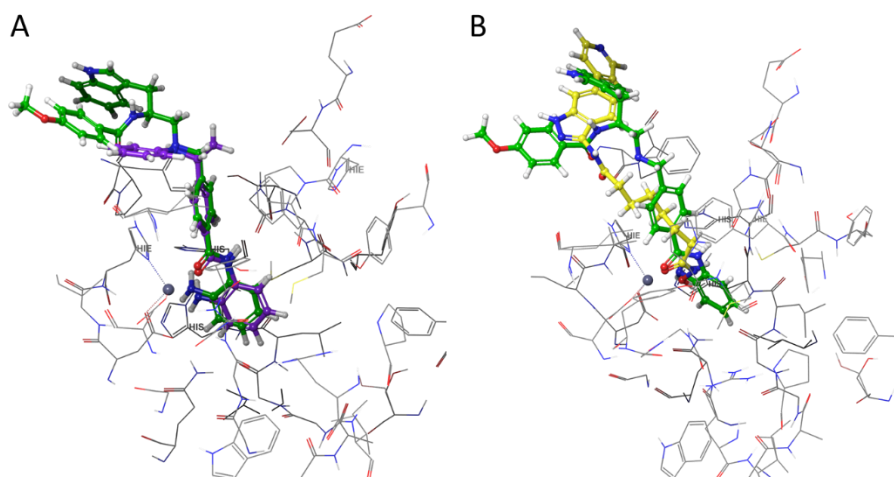


**Figure 6: A; comparison between two benzamide compounds with different rim groups, B; comparison between hydroxamic acid compound and benzamide**

Another important factor is the presence of a hydrophobic aromatic ring within the hydrophobic channel as predicted by both the hydrophobic and aromatic ring similarity fields of the model. Figure 7 illustrates this by comparing two benzamide compounds from a previous study by Li et al. [40] with the same chemical structure, bar the linker being a phenyl ring in the first one (cyan skeleton,  $IC_{50} = 157$  nM), and an alkyl chain in the second (orange skeleton,  $IC_{50} = 296$  nM).

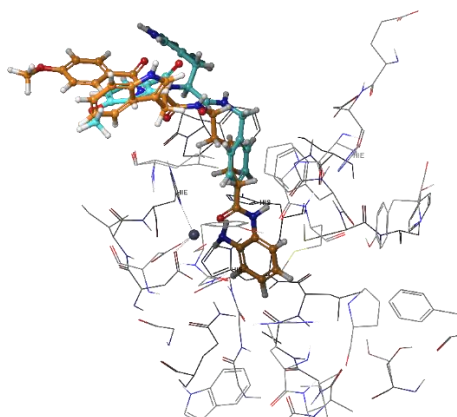


**Figure 7: comparison between two benzamide compounds with different linker groups**

Going back to figure 6B, the hydroxamic acid compound contains an alkyl linker as opposed to the benzamide with the phenyl linker, which should mean higher potency for the benzamide compound, however, this disparity only affects experimental activity ever so slightly, which further shows the importance of the steric similarity field over other fields, as both compounds have large bulky groups similarly positioned at the active site rim, and thus aren't significantly affected with changes in other similarity field interactions.

These findings could help design novel potent HDAC2 inhibitors by using large bulky groups that can be positioned within the rim of the active site, together with a hydrophobic aromatic ring as the linker that resides within the hydrophobic channel.

#### 4. Conclusion:

A 3D-QSAR model was developed for predicting the activity of HDAC2 inhibitors using a modified CoMSIA approach. The model was generated using a training set of 85 compounds, and validated using a test set of 34 compounds, and further using an independent external validation set of 49 compounds, all selected from relevant studies and literature. The sets encompassed a wide array of chemical structures, with different experimental inhibitory activities spanning multiple orders of magnitude. The generated model conformed to all required parameters and exhibited good predictivity and stability. The model predicts that the presence of a large bulky group at the rim of the active site, as well as a hydrophobic aromatic ring in the hydrophobic channel significantly improve inhibitory activity against HDAC2. These findings could prove useful in designing novel potent HDAC2 inhibitors.

#### References:

- Porter, N. J., & Christianson, D. W. (2019). Structure, mechanism, and inhibition of the zinc-dependent histone deacetylases. *Current Opinion in Structural Biology*, 59, 9–18. <https://doi.org/10.1016/j.sbi.2019.02.001>
- Ho, T. C. S., Chan, A. H. Y., & Ganesan, A. (2020). Thirty years of HDAC inhibitors: 2020 insight and hindsight. *Journal of Medicinal Chemistry*, 63(21), 12460–12484. <https://doi.org/10.1021/acs.jmedchem.0c00628>
- Milazzo, G., Mercatelli, D., Di Muzio, G., Triboli, L., De Rosa, P., Perini, G., & et al. (2020). Histone deacetylases (HDACs): Evolution, specificity, role in transcriptional complexes, and pharmacological actionability. *Genes*, 11(5), 556. <https://doi.org/10.3390/genes11050556>
- Shetty, M. G., Pai, P., Deaver, R. E., Satyamoorthy, K., & Babitha, K. S. (2021). Histone deacetylase 2 selective inhibitors: A versatile therapeutic strategy as next generation drug target in cancer therapy. *Pharmacological Research*, 170, 105695. <https://doi.org/10.1016/j.phrs.2021.105695>
- Gediya, P., Parikh, P. K., Vyas, V. K., & Ghatge, M. D. (2021). Histone deacetylase 2: A potential therapeutic target for cancer and neurodegenerative disorders. *European Journal of Medicinal Chemistry*, 216, 113332. <https://doi.org/10.1016/j.ejmech.2021.113332>
- Kaler, P., Sasazuki, T., Shirasawa, S., Augenlicht, L., & Klampfer, L. (2008). HDAC2 deficiency sensitizes colon cancer cells to TNF $\alpha$ -induced apoptosis through inhibition of NF- $\kappa$ B activity. *Experimental Cell Research*, 314(7), 1507–1518. <https://doi.org/10.1016/j.yexcr.2007.12.025>
- Noh, J. H., Jung, K. H., Kim, J. K., Eun, J. W., Bae, H. J., Xie, H. J., & et al. (2011). Aberrant regulation of HDAC2 mediates proliferation of hepatocellular carcinoma cells by deregulating expression of G1/S cell cycle proteins. *PLOS ONE*, 6(11), e28103. <https://doi.org/10.1371/journal.pone.0028103>
- Kim, J. K., Noh, J. H., Eun, J. W., Jung, K. H., Bae, H. J., Shen, Q., & et al. (2013). Targeted inactivation of HDAC2 restores p16INK4a activity and exerts antitumor effects on human gastric cancer. *Molecular Cancer Research*, 11(1), 62–73. <https://doi.org/10.1158/1541-7786.MCR-12-0404>
- Guan, J. S., Haggarty, S. J., Giacometti, E., Dannenberg, J. H., Joseph, N., Gao, J., & et al. (2009). HDAC2 negatively regulates memory formation and synaptic plasticity. *Nature*, 459(7243), 55–60. <https://doi.org/10.1038/nature07925>

10. Ganai, S. A., Abdullah, E., Rashid, R., & Altaf, M. (2017). Combinatorial in silico strategy towards identifying potential hotspots during inhibition of structurally identical HDAC1 and HDAC2 enzymes for effective chemotherapy against neurological disorders. *Frontiers in Molecular Neuroscience*, 10, 357. <https://doi.org/10.3389/fnmol.2017.00357>
11. Trivedi, C. M., Luo, Y., Yin, Z., Zhang, M., Zhu, W., Wang, T., et al. (2007). Hdac2 regulates the cardiac hypertrophic response by modulating Gsk3 beta activity. *Nature Medicine*, 13(3), 324–331.
12. Sandonà, M., Cavioli, G., Renzini, A., Cedola, A., Gigli, G., Coletti, D., et al. (2023). Histone deacetylases: Molecular mechanisms and therapeutic implications for muscular dystrophies. *International Journal of Molecular Sciences*, 24(5).
13. Di Micco, S., Chini, M. G., Terracciano, S., Bruno, I., Riccio, R., & Bifulco, G. (2013). Structural basis for the design and synthesis of selective HDAC inhibitors. *Bioorganic & Medicinal Chemistry*, 21(13), 3795–3807.
14. Melesina, J., Simoben, C. V., Praetorius, L., Bülbül, E. F., Robaa, D., & Sippl, W. (2021). Strategies to design selective histone deacetylase inhibitors. *ChemMedChem*, 16(9), 1336–1359.
15. Ruzic, D., Djokovic, N., Srdic-Rajic, T., Echeverria, C., Nikolic, K., & Santibanez, J. F. (2022). Targeting histone deacetylases: Opportunities for cancer treatment and chemoprevention. *Pharmaceutics*, 14.
16. Zhang, C. L., McKinsey, T. A., Chang, S., Antos, C. L., Hill, J. A., & Olson, E. N. (2002). Class II histone deacetylases act as signal-responsive repressors of cardiac hypertrophy. *Cell*, 110(4), 479–488.
17. Antos, C. L., McKinsey, T. A., Dreitz, M., Hollingsworth, L. M., Zhang, C. L., Schreiber, K., et al. (2003). Dose-dependent blockade to cardiomyocyte hypertrophy by histone deacetylase inhibitors. *Journal of Biological Chemistry*, 278(31), 28930–28937.
18. Roy, K., Kar, S., & Das, R. N. (2015). Chapter 8 - Introduction to 3D-QSAR. In K. Roy, S. Kar, & R. N. Das (Eds.), *Understanding the basics of QSAR for applications in pharmaceutical sciences and risk assessment* (pp. 291–317). Boston: Academic Press.
19. Silakari, O., & Singh, P. K. (2021). Chapter 2 - QSAR: Descriptor calculations, model generation, validation and their application. In O. Silakari & P. K. Singh (Eds.), *Concepts and experimental protocols of modelling and informatics in drug design* (pp. 29–63). Academic Press.
20. Klebe, G. (2002). Comparative molecular similarity indices analysis: CoMSIA (pp. 87–104).
21. Schrödinger Release 2023-1: Prime. Schrödinger, LLC, New York, NY, 2023.
22. Schrödinger Release 2023-1: LigPrep. Schrödinger, LLC, New York, NY, 2023.
23. Schrödinger Release 2023-1: Glide. Schrödinger, LLC, New York, NY, 2023.
24. Schrödinger Release 2023-1: Force Fields. Schrödinger, LLC, New York, NY, 2023.
25. The Worldwide Protein Data Bank archive. Retrieved from <http://www.wwpdb.org/>
26. The RCSB online database. Retrieved from <http://www.rcsb.org/>
27. Berman, H., Henrick, K., & Nakamura, H. (2003). Announcing the worldwide Protein Data Bank. *Nature Structural & Molecular Biology*, 10(12), 980.
28. Berman, H. M., Westbrook, J., Feng, Z., Gilliland, G., Bhat, T. N., Weissig, H., et al. (2000). The Protein Data Bank. *Nucleic Acids Research*, 28(1), 235–242.

29. Lu, C., Wu, C., Ghoreishi, D., Chen, W., Wang, L., Damm, W., et al. (2021). OPLS4: Improving force field accuracy on challenging regimes of chemical space. *Journal of Chemical Theory and Computation*, 17(7), 4291–4300.
30. Deschamps, N., Simões-Pires, C. A., Carrupt, P.-A., & Nurisso, A. (2015). How the flexibility of human histone deacetylases influences ligand binding: An overview. *Drug Discovery Today*, 20(6), 736–742.
31. Luo, Y., & Li, H. (2020). Structure-based inhibitor discovery of class I histone deacetylases (HDACs). *International Journal of Molecular Sciences*, 21\*(22). <https://doi.org/10.3390/ijms21228485>
32. Sherman, W., Beard, H. S., & Farid, R. (2006). Use of an induced fit receptor structure in virtual screening. *Chemistry & Biology Drug Design*, 67\*(1), 83–84. <https://doi.org/10.1111/j.1747-0285.2006.00378.x>
33. Methot, J. L., Chakravarty, P. K., Chenard, M., Close, J., Cruz, J. C., Dahlberg, W. K., et al. (2008). Exploration of the internal cavity of histone deacetylase (HDAC) with selective HDAC1/HDAC2 inhibitors (SHI-1:2). *Bioorganic & Medicinal Chemistry Letters*, 18\*(3), 973–978. <https://doi.org/10.1016/j.bmcl.2007.11.081>
34. Tropsha, A., Gramatica, P., & Gombar, V. (2003). The importance of being earnest: Validation is the absolute essential for successful application and interpretation of QSPR models. *QSAR & Combinatorial Science*, 22\*(1), 69–77. <https://doi.org/10.1002/qsar.200390007>
35. Tropsha, A., & Golbraikh, A. (2007). Predictive QSAR modeling workflow, model applicability domains, and virtual screening. *Current Pharmaceutical Design*, 13\*(34), 3494–3504. <https://doi.org/10.2174/138161207782794877>
36. Tropsha, A. (2010). Best practices for QSAR model development, validation, and exploitation. *Molecular Informatics*, 29\*(6–7), 476–488. <https://doi.org/10.1002/minf.201000061>
37. Marson, C. M., Matthews, C. J., Atkinson, S. J., Lamadema, N., & Thomas, N. S. (2015). Potent and selective inhibitors of histone deacetylase-3 containing chiral oxazoline capping groups and a N-(2-aminophenyl)-benzamide binding unit. *Journal of Medicinal Chemistry*, 58\*(17), 6803–6818. <https://doi.org/10.1021/acs.jmedchem.5b00808>
38. Marson, C. M., Matthews, C. J., Yiannaki, E., Atkinson, S. J., Soden, P. E., Shukla, L., et al. (2013). Discovery of potent, isoform-selective inhibitors of histone deacetylase containing chiral heterocyclic capping groups and a N-(2-aminophenyl)benzamide binding unit. *Journal of Medicinal Chemistry*, 56\*(15), 6156–6174. <https://doi.org/10.1021/jm400656k>
39. Bressi, J. C., Jennings, A. J., Skene, R., Wu, Y., Melkus, R., De Jong, R., et al. (2010). Exploration of the HDAC2 foot pocket: Synthesis and SAR of substituted N-(2-aminophenyl)benzamides. *Bioorganic & Medicinal Chemistry Letters*, 20\*(10), 3142–3145. <https://doi.org/10.1016/j.bmcl.2010.03.068>
40. Li, X., Zhang, Y., Jiang, Y., Wu, J., Inks, E. S., Chou, C. J., et al. (2017). Selective HDAC inhibitors with potent oral activity against leukemia and colorectal cancer: Design, structure-activity relationship, and anti-tumor activity study. *European Journal of Medicinal Chemistry*, 134\*, 185–206. <https://doi.org/10.1016/j.ejmech.2017.04.034>
41. Vaidya, A. S., Karumudi, B., Mendonca, E., Madriaga, A., Abdelkarim, H., Van Breemen, R. B., et al. (2012). Design, synthesis, modeling, biological evaluation, and

- photoaffinity labeling studies of novel series of photoreactive benzamide probes for histone deacetylase 2. *Bioorganic & Medicinal Chemistry Letters*, 22\*(15), 5025–5030. <https://doi.org/10.1016/j.bmcl.2012.06.085>
42. Cao, F., Zwinderman, M. R. H., Van Merkerk, R., Ettema, P. E., Quax, W. J., & Dekker, F. J. (2019). Inhibitory selectivity among class I HDACs has a major impact on inflammatory gene expression in macrophages. *European Journal of Medicinal Chemistry*, 177\*, 457–466. <https://doi.org/10.1016/j.ejmech.2019.05.076>
43. Zhang, L., Li, X., Chen, Y., Wan, M., Jiang, Q., Zhang, L., et al. (2019). Discovery of N-(2-Aminophenyl)-4-(bis(2-chloroethyl)amino)benzamide as a potent histone deacetylase inhibitor. *Frontiers in Pharmacology*, 10\*, 957. <https://doi.org/10.3389/fphar.2019.00957>
44. Krieger, V., Hamacher, A., Cao, F., Stenzel, K., Gertzen, C. G. W., Schäker-Hübner, L., et al. (2019). Synthesis of peptoid-based class I-selective histone deacetylase inhibitors with chemosensitizing properties. *Journal of Medicinal Chemistry*, 62\*(24), 11260–11279. <https://doi.org/10.1021/acs.jmedchem.9b01465>
45. Cai, J., Wei, H., Hong, K. H., Wu, X., Zong, X., Cao, M., et al. (2015). Discovery, bioactivity, and docking simulation of Vorinostat analogues containing 1,2,4-oxadiazole moiety as potent histone deacetylase inhibitors and antitumor agents. *Bioorganic & Medicinal Chemistry*, 23\*(13), 3457–3471. <https://doi.org/10.1016/j.bmc.2015.04.049>
46. Liu, J., Zhou, J., He, F., Gao, L., Wen, Y., & Gao, L. (2020). Design, synthesis, and biological evaluation of novel indazole-based derivatives as potent HDAC inhibitors via fragment-based virtual screening. *European Journal of Medicinal Chemistry*, 192\*, 112189. <https://doi.org/10.1016/j.ejmech.2020.112189>
47. Cai, J., Wei, H., Hong, K. H., Wu, X., Cao, M., Zong, X., et al. (2015). Discovery and preliminary evaluation of 2-aminobenzamide and hydroxamate derivatives containing 1,2,4-oxadiazole moiety as potent histone deacetylase inhibitors. *European Journal of Medicinal Chemistry*, 96\*, 1–13. <https://doi.org/10.1016/j.ejmech.2015.04.016>
48. Taha, T. Y., Aboukhatwa, S. M., Knopp, R. C., Ikegaki, N., Abdelkarim, H., Neerasa, J., et al. (2017). Design, synthesis, and biological evaluation of tetrahydroisoquinoline-based histone deacetylase 8 selective inhibitors. *ACS Medicinal Chemistry Letters*, 8\*(8), 824–829. <https://doi.org/10.1021/acsmedchemlett.7b00195>
49. Yang, J., Cheng, G., Xu, Q., Luan, S., Wang, S., Liu, D., et al. (2018). Design, synthesis, and biological evaluation of novel hydroxamic acid-based histone deacetylase 6 selective inhibitors bearing phenylpyrazol scaffold as surface recognition motif. *Bioorganic & Medicinal Chemistry*, 26\*(8), 1418–1425. <https://doi.org/10.1016/j.bmc.2018.02.012>
50. Moradei, O. M., Mallais, T. C., Frechette, S., Paquin, I., Tessier, P. E., Leit, S. M., et al. (2007). Novel aminophenyl benzamide-type histone deacetylase inhibitors with enhanced potency and selectivity. *Journal of Medicinal Chemistry*, 50\*(23), 5543–5546. <https://doi.org/10.1021/jm070489v>
51. Zang, J., Shi, B., Liang, X., Gao, Q., Xu, W., & Zhang, Y. (2017). Development of N-hydroxycinnamamide-based HDAC inhibitors with improved HDAC inhibitory activity and in vitro antitumor activity. *Bioorganic & Medicinal Chemistry*, 25\*(9), 2666–2675. <https://doi.org/10.1016/j.bmc.2017.02.058>
52. Pan, T., Dan, Y., Guo, D., Jiang, J., Ran, D., Zhang, L., et al. (2021). Discovery of 2,4-pyrimidinediamine derivatives as potent dual inhibitors of ALK and HDAC.

- \*European Journal of Medicinal Chemistry, 224\*, 113672.  
<https://doi.org/10.1016/j.ejmech.2021.113672>
53. Liu, J., Zhu, Y., He, Y., Zhu, H., Gao, Y., Li, Z., et al. (2019). Combined pharmacophore modeling, 3D-QSAR, and docking studies to identify novel HDAC inhibitors using drug repurposing. \*Journal of Biomolecular Structure and Dynamics, 38\*, 1–15. <https://doi.org/10.1080/07391102.2019.1595181>
54. Abdizadeh, R., Hadizadeh, F., & Abdizadeh, T. (2019). QSAR analysis of coumarin-based benzamides as histone deacetylase inhibitors using CoMFA, CoMSIA, and HQSAR methods. \*Journal of Molecular Structure, 1199\*, 126961. <https://doi.org/10.1016/j.molstruc.2019.126961>